Dipole moment and intensities in the electronic ground state of NH_3: Bridging the gap between *ab initio* theory and spectroscopic experiment.

S.N. Yurchenko,[1] M. Carvajal,[2] W. Thiel,[1] Hai Lin,[3] and Per Jensen[4]

[1]*Max-Planck-Institut für Kohlenforschung, Kaiser-Wilhelm-Platz 1, D–45470 Mülheim an der Ruhr, Germany*

[2]*Departamento de Fisica Aplicada, Facultad de Ciencias Experimentales, Avda. de las FF.AA. s/n, Universidad de Huelva, 21071, Huelva, Spain*

[3]*Department of Chemistry, University of Minnesota, 207, Pleasant St. SE. Minneapolis, Minnesota 55455, U.S.A.*

[4]*FB C – Theoretische Chemie, Bergische Universität, D–42097 Wuppertal, Germany.*

(Dated: December 10, 2004)

Abstract

We report here theoretical values for the transition moments of an extensive set of vibrational bands in the electronic ground state of $^{14}NH_3$. For selected bands, we have further made detailed simulations of the rotational structure. The calculations are carried out by means of recently developed computational procedures for describing the nuclear motion and are based on a high-level *ab initio* potential energy surface, and high-level dipole moment surfaces, for the electronic ground state of NH_3. The reported theoretical intensity values are compared to, and found to agree very well with, corresponding experimental results. It is believed that the computational method, in conjunction with high-quality *ab initio* potential energy and dipole moment surfaces, can simulate rotation-vibration spectra of XY_3 pyramidal molecules prior to observation with sufficient accuracy to facilitate the observation of these spectra. By degrading the accuracy of selected elements of the calculations, we have also investigated the influence of customary approximations on the computed intensity values.

Contents

I. INTRODUCTION

Modern *ab initio* calculations of molecular potential energy surfaces, coupled with high-level treatments of the nuclear motion, provide very accurate descriptions of the properties of isolated molecules. In particular, the theoretical calculations often yield molecular energy levels in very good agreement with the results of spectroscopic experiments. One could think that owing to the progress in theoretical methods, the assignment of molecular spectra would become increasingly trivial: The spectrum, or at least the transition frequencies, can be predicted from first principles with sufficient accuracy that the assignment of each individual transition can be straightforwardly obtained from the theoretical calculation. There are

examples, such as the water molecule [1, 2], where such a 'first-principles assignment' can be made, but present-day assignment of spectra is still largely based on the more traditional methods of general pattern recognition, search for combination differences, and the least-squares fitting of the frequencies for the assigned transitions, with subsequent prediction of the frequencies for unassigned lines, by means of models involving effective rotation-vibration parameters (see, for example, Ref. [3]).

In recent papers [4–8] we have described the development and application of a theoretical model for simulating rotation-vibration spectra for isolated electronic states of XY_3 pyramidal molecules. The applications, so far, have been to the NH_3 [4, 6, 8] and PH_3 [5, 7] molecules. Initially [4, 6], we developed a computational procedure for calculating rotation-vibration energies and wavefunctions of XY_3 molecules from an *ab initio* potential energy surface. With energies for $^{14}NH_3$, obtained with this procedure from a high-quality *ab initio* potential energy surface [4, 9], we were able to assist the assignment of high-resolution molecular spectra, in that we could verify – for the most part – the tentative assignment to the $4\nu_2^+$ band [10] of 55 weak transitions observed in an experimental study of the ν_1, ν_3, and $2\nu_4$ bands of $^{14}NH_3$.

Our theoretical model for the rotation and vibration of an XY_3 molecule (for details, see [6]) is a variational (i.e., perturbation-theory-free) implementation of the Hougen-Bunker-Johns (henceforth: HBJ) approach [11, 12]. The HBJ approach is designed to provide maximum separation of the rotational and vibrational motions in the quantum-mechanical description, and so our model is particularly suitable for calculating the energies and wavefunctions of highly excited rotational states. So, in [7], we could generate energies and wavefunctions for states with $J \leq 80$ in the vibrational ground state of PH_3 and study the formation of six-fold clusters of rotational energies; these clusters are analogous to the four-fold clusters extensively discussed for XH_2 molecules (see [12, 13] and references therein).

Since we can treat highly excited rotational states of XY_3 molecules, we can generate the energies and wavefunctions necessary to simulate realistic rotation-vibration spectra of them. Such simulations obviously help 'bridging the gap' between *ab initio* theory and experimental spectroscopy; they are a prerequisite for the 'first-principles assignments' mentioned above. We have described in [8] the extension of our theoretical model to the computation of line strengths (see below) and intensities for electric dipole transitions within an isolated electronic state of an XY_3 pyramidal molecule. Reference [8] also reported the calculation

of *ab initio* dipole moment surfaces for the electronic ground state of $^{14}NH_3$ together with initial applications of the new intensity model to $^{14}NH_3$ rotation-vibration transitions; in the present work we extend these calculations and, by comparing our computed intensities with the results of more approximate treatments, we make a critical assessment of various approximations customarily made in intensity calculations. For a detailed discussion of the theoretical description of the molecular rotation-vibration motion and the intensities of the associated transitions, the reader is referred to Refs. [6] and [8], respectively. The present work gives only a brief outline of the theory, intended to provide the reader with sufficient information for understanding the origin of the results that we present.

One purpose of the present paper is to determine the degree of agreement with experiment that can be obtained in 'pure' *ab initio* calculations of molecular intensities. In consequence, our calculations are based on a potential energy surface and dipole moment surfaces obtained directly from *ab initio* calculations: We have made no adjustments to fit experimental data for NH_3.

II. THE MOLECULAR DIPOLE MOMENT

A. The *ab initio* calculation

As discussed in [8], the *ab initio* dipole moment values employed in the present work were computed with the MOLPRO2000 [14, 15] package at the CCSD(T)/aug-cc-pVTZ level of theory (i.e., coupled cluster theory with all single and double substitutions [16] and a perturbative treatment of connected triple excitations [17, 18] with the augmented correlation-consistent triple-zeta basis [19, 20]) in the frozen-core approximation. Dipole moments were computed in a numerical finite-difference procedure with an added external dipole field of 0.005 a.u. The convergence thresholds were 10^{-10} for density and 10^{-7} a.u. for energy in Hartree-Fock (HF) calculations, and 10^{-10} a.u. for energy and 10^{-10} for coefficients in CCSD(T) computations.

The dipole moment *ab initio* surface used in the present study has been determined on a six-dimensional grid (the 6D-1 grid in Ref. [4]) consisting of 14,400 unique geometries that form a regular grid in the range 0.85 Å $\leq r_1 \leq r_2 \leq r_3 \leq$ 1.20 Å and $80° \leq \alpha_1, \alpha_2, \alpha_3 \leq 120°$. Here, r_i is the instantaneous value of the internuclear distance N–H_i, $i = 1, 2, 3$, and

FIG. 1: The labeling of the nuclei, the molecule-fixed axis system xyz, and selected coordinates employed for NH_3 (see text).

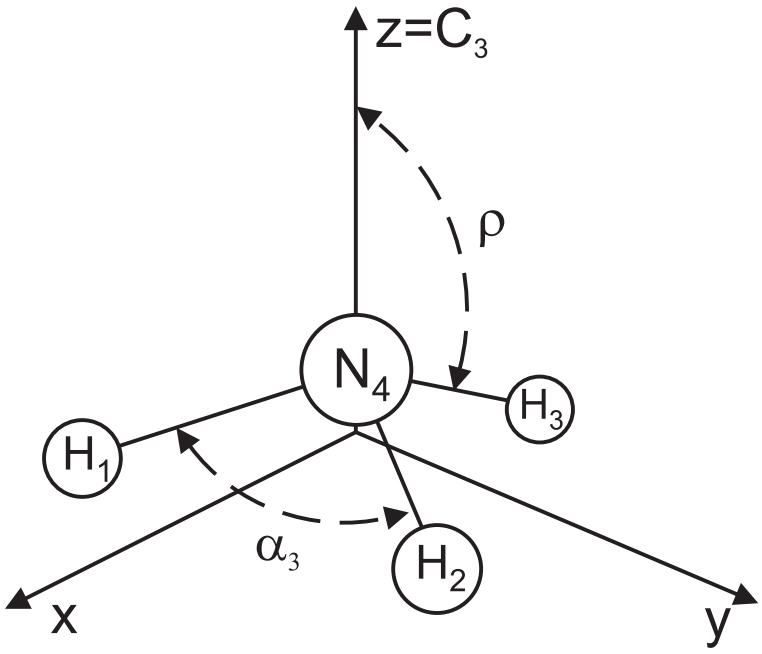

the bond angles are given as $\alpha_1 = \angle(H_2PH_3)$, $\alpha_2 = \angle(H_1PH_3)$, and $\alpha_3 = \angle(H_1PH_2)$ [see Fig. 1].

In the *ab initio* calculations the components of the molecular dipole moment are given in a right-handed Cartesian axis system $x'y'z'$ with origin in the nitrogen nucleus. The H_1 nucleus lies on the z' axis with a positive value of the z' coordinate, and the $y'z'$ plane is defined by the nitrogen nucleus and the protons H_1 and H_2.

B. A general analytical representation of the dipole moment

In the so-called Molecular Bond (MB) representation [8, 21, 22], the electronically averaged dipole moment vector $\bar{\boldsymbol{\mu}}$ [8, 12] for NH_3 is given by

$$\bar{\boldsymbol{\mu}} = \bar{\mu}_1^{\mathrm{Bond}}\,\mathbf{e}_1 + \bar{\mu}_2^{\mathrm{Bond}}\,\mathbf{e}_2 + \bar{\mu}_3^{\mathrm{Bond}}\,\mathbf{e}_3 \tag{2.1}$$

where the three functions $\bar{\mu}_i^{\mathrm{Bond}}$, $i = 1, 2, 3$, depend on the vibrational coordinates, and $\mathbf{e}_i$ is the unit vector along the N–H_i bond,

$$\mathbf{e}_i = \frac{\mathbf{r}_i - \mathbf{r}_4}{|\mathbf{r}_i - \mathbf{r}_4|} \tag{2.2}$$

with $\mathbf{r}_i$ as the position vector of nucleus i (the protons are labeled 1, 2, 3, and the nitrogen nucleus is labeled 4, see Fig. 1) in the axis system $x'y'z'$ defined above. As discussed in [8], the representation of $\bar{\boldsymbol{\mu}}$ in Eq. (2.1) is 'body-fixed' in the sense that it relates the dipole moment vector directly to the instantaneous positions of the nuclei (i.e., to the vectors $\mathbf{r}_i$). In consequence, we can use Eq. (2.1) to obtain the coordinates of $\bar{\boldsymbol{\mu}}$ in any axis system.

Our implementation of the MB representation for the electronic-ground-state dipole moment of NH_3 is detailed in [8]; here we give only a brief outline. We express the three functions $\bar{\mu}_i^{\rm Bond}$, $i = 1, 2, 3$, as

$$\bar{\mu}_i^{\rm Bond} = \sum_{j=1}^{3} \left(\mathbf{A}^{-1}\right)_{ij} \left(\bar{\boldsymbol{\mu}} \cdot \mathbf{e}_j\right) \tag{2.3}$$

where $(\mathbf{A}^{-1})_{ij}$ is an element of the non-orthogonal 3×3 matrix $\mathbf{A}^{-1}$ obtained as the inverse of

$$\mathbf{A} = \begin{pmatrix} 1 & \cos\alpha_3 & \cos\alpha_2 \\ \cos\alpha_3 & 1 & \cos\alpha_1 \\ \cos\alpha_2 & \cos\alpha_1 & 1 \end{pmatrix}. \tag{2.4}$$

When the molecule is planar, i.e., when $\alpha_1 + \alpha_2 + \alpha_3 = 2\pi$, the determinant $|\mathbf{A}| = 0$ and $\mathbf{A}$ cannot be inverted. For planar geometries $\mathbf{e}_1$, $\mathbf{e}_2$, and $\mathbf{e}_3$ are linearly dependent and there are infinitely many possible values of $(\bar{\mu}_1^{\rm Bond}, \bar{\mu}_2^{\rm Bond}, \bar{\mu}_3^{\rm Bond})$. In this case we set $\bar{\mu}_3^{\rm Bond} = 0$ in Eq. (2.1) and express $\bar{\boldsymbol{\mu}}$ in terms of $\mathbf{e}_1$ and $\mathbf{e}_2$ only, i.e., we determine $\bar{\mu}_1^{\rm Bond}$ and $\bar{\mu}_2^{\rm Bond}$ in terms of $\bar{\mu}_1$ and $\bar{\mu}_2$.

We have shown in [8] that the projections $\bar{\boldsymbol{\mu}} \cdot \mathbf{e}_j$, $j = 1, 2, 3$, in Eq. (2.3) can be expressed in terms of the geometrically defined coordinates r_1, r_2, r_3, α_1, α_2, and α_3. By utilizing that a permutation of the protons in NH_3 does not change the molecular dipole moment [12] we further derived [8] that all three projections are given in terms of a single function $\bar{\mu}_0(r_1, r_2, r_3, \alpha_1, \alpha_2, \alpha_3)$:

$$\bar{\boldsymbol{\mu}} \cdot \mathbf{e}_1 = \bar{\mu}_0(r_1, r_2, r_3, \alpha_1, \alpha_2, \alpha_3) = \bar{\mu}_0(r_1, r_3, r_2, \alpha_1, \alpha_3, \alpha_2), \tag{2.5}$$

$$\bar{\boldsymbol{\mu}} \cdot \mathbf{e}_2 = \bar{\mu}_0(r_2, r_3, r_1, \alpha_2, \alpha_3, \alpha_1) = \bar{\mu}_0(r_2, r_1, r_3, \alpha_2, \alpha_1, \alpha_3), \tag{2.6}$$

$$\bar{\boldsymbol{\mu}} \cdot \mathbf{e}_3 = \bar{\mu}_0(r_3, r_1, r_2, \alpha_3, \alpha_1, \alpha_2) = \bar{\mu}_0(r_3, r_2, r_1, \alpha_3, \alpha_2, \alpha_1). \tag{2.7}$$

This function is expressed as an expansion

$$\bar{\mu}_0 = \sum_k \mu_k^{(0)} \xi_k$$

$$+ \sum_{k,l} \mu^{(0)}_{k,l} \xi_k \xi_l + \sum_{k,l,m} \mu^{(0)}_{k,l,m} \xi_k \xi_l \xi_m + \sum_{k,l,m,n} \mu^{(0)}_{k,l,m,n} \xi_k \xi_l \xi_m \xi_n + \ldots , \tag{2.8}$$

in the variables

$$\xi_k \;=\; r_k \exp\left(-\beta^2 \, r_k^2\right) , \quad k = 1, 2, 3, \tag{2.9}$$

$$\xi_l \;=\; \cos\left(\alpha_{l-3}\right) - \cos\left(\frac{2\pi}{3}\right) = \frac{1}{2} + \cos\left(\alpha_{l-3}\right) , \quad l = 4, 5, 6, \tag{2.10}$$

which are chosen such that $\bar{\mu}_0 = 0$ for ($r_1 = r_2 = r_3 = 0$, $\alpha_1 = \alpha_2 = \alpha_3 = 2\pi/3$). Following Ref. [22], we have introduced the factor $\exp\left(-\beta^2 r_k^2\right)$ in order to keep the expansion in Eq. (2.8) from diverging at large r_i.

The function $\bar{\mu}_0(r_1, r_2, r_3, \alpha_1, \alpha_2, \alpha_3)$ is invariant to the simultaneous interchanges $r_2 \leftrightarrow r_3$ and $\alpha_2 \leftrightarrow \alpha_3$ [Eq. (2.5)] and, therefore, the expansion coefficients $\mu^{(0)}_k$, $\mu^{(0)}_{k,l}$, $\mu^{(0)}_{k,l,m}$, and $\mu^{(0)}_{k,l,m,n}$ in Eq. (2.8) are subject to constraints. In general, we have

$$\mu^{(0)}_{k',l',m',\ldots} = \mu^{(0)}_{k,l,m,\ldots} \tag{2.11}$$

if the indices $k', l', m', \ldots$ are obtained from $k, l, m, \ldots$ by replacing all indices 2 by 3, all indices 3 by 2, all indices 5 by 6, and all indices 6 by 5. For instance, $\mu^{(0)}_2 = \mu^{(0)}_3$, $\mu^{(0)}_5 = \mu^{(0)}_6$, $\mu^{(0)}_{2,2} = \mu^{(0)}_{3,3}$, $\mu^{(0)}_{5,5} = \mu^{(0)}_{6,6}$, $\mu^{(0)}_{1,2,2} = \mu^{(0)}_{1,3,3}$, and $\mu^{(0)}_{1,2,6} = \mu^{(0)}_{1,3,5}$.

We have determined the values of the expansion parameters in Eq. (2.8), which we take to fourth order, in a least-squares fitting to the 3×14440 *ab initio* dipole moment projections $\bar{\boldsymbol{\mu}} \cdot \mathbf{e}_j$, j = 1, 2, 3, calculated *ab initio* for NH_3 at the CCSD(T)/aug-cc-pVTZ level of theory (Section II A). Details of this fitting are given in [8]. We could usefully vary 91 parameters in the final fitting, which had a root-mean-square (rms) deviation of 0.0006 D. Table I lists the optimized parameter values. Parameters, whose absolute values were determined to be less than their standard errors in initial fittings, were constrained to zero in the final fitting and omitted from the table. Furthermore, we give in the table only one member of each parameter pair related by Eq. (2.11).

As already reported in Ref. [4], the ATZfc dipole moment surface gives rise to an 'equilibrium' moment of μ_e = 1.5198 D at the ATZfc *ab initio* equilibrium geometry of $r_1 = r_2 = r_3 = r_e$ = 1.0149 Å and $\alpha_1 = \alpha_2 = \alpha_3 = \alpha_e$ = 106.4°. The experimental value for μ_e is (1.561±0.005) D [23].

TABLE I: MB-representation dipole moment parameters (in D unless otherwise indicated) for the electronic ground state of NH_3.

Parameter	Value	Parameter	Value	Parameter	Value
β/Å^{-1}	1.0928(15)[a]	$\mu^{(0)}_{225}$	-2.04(17)	$\mu^{(0)}_{1456}$	3.019(94)
$\mu^{(0)}_{1}$	8.7(13)	$\mu^{(0)}_{226}$	8.95(15)	$\mu^{(0)}_{1466}$	-0.5794(93)
$\mu^{(0)}_{3}$	-4.632(66)	$\mu^{(0)}_{234}$	-1.961(19)	$\mu^{(0)}_{1566}$	0.5262(76)
$\mu^{(0)}_{4}$	0.218(11)	$\mu^{(0)}_{246}$	2.967(17)	$\mu^{(0)}_{1666}$	1.3038(73)
$\mu^{(0)}_{5}$	0.5155(71)	$\mu^{(0)}_{256}$	1.36(20)	$\mu^{(0)}_{2222}$	76.4(89)
$\mu^{(0)}_{11}$	-43.75(74)	$\mu^{(0)}_{266}$	3.421(22)	$\mu^{(0)}_{2224}$	7.46(17)
$\mu^{(0)}_{13}$	-4.96(25)	$\mu^{(0)}_{333}$	-73.52(94)	$\mu^{(0)}_{2225}$	6.49(20)
$\mu^{(0)}_{14}$	3.219(80)	$\mu^{(0)}_{334}$	-2.1(15)	$\mu^{(0)}_{2245}$	-3.135(20)
$\mu^{(0)}_{16}$	8.196(51)	$\mu^{(0)}_{344}$	0.4884(76)	$\mu^{(0)}_{2246}$	-1.734(26)
$\mu^{(0)}_{23}$	0.416(38)	$\mu^{(0)}_{444}$	0.3513(60)	$\mu^{(0)}_{2255}$	0.5(22)
$\mu^{(0)}_{33}$	29.71(37)	$\mu^{(0)}_{445}$	0.3849(30)	$\mu^{(0)}_{2256}$	-1.061(39)
$\mu^{(0)}_{34}$	-0.196(46)	$\mu^{(0)}_{466}$	0.4947(35)	$\mu^{(0)}_{2266}$	-2.639(35)
$\mu^{(0)}_{35}$	-5.29(45)	$\mu^{(0)}_{556}$	-0.053(34)	$\mu^{(0)}_{2335}$	3.76(18)
$\mu^{(0)}_{36}$	0.554(53)	$\mu^{(0)}_{1111}$	-93.6(15)	$\mu^{(0)}_{2336}$	-2.45(17)
$\mu^{(0)}_{44}$	-0.526(49)	$\mu^{(0)}_{1114}$	4.84(27)	$\mu^{(0)}_{2345}$	2.723(27)
$\mu^{(0)}_{46}$	-0.4327(47)	$\mu^{(0)}_{1115}$	11.91(18)	$\mu^{(0)}_{2356}$	-2.866(85)
$\mu^{(0)}_{55}$	-0.196(38)	$\mu^{(0)}_{1122}$	9.7(59)	$\mu^{(0)}_{2366}$	-0.954(41)
$\mu^{(0)}_{56}$	0.6815(82)	$\mu^{(0)}_{1124}$	-2.62(14)	$\mu^{(0)}_{2444}$	-0.2227(69)
$\mu^{(0)}_{111}$	97.5(17)	$\mu^{(0)}_{1126}$	-1.802(45)	$\mu^{(0)}_{2456}$	-1.0261(55)
$\mu^{(0)}_{112}$	1.73(34)	$\mu^{(0)}_{1136}$	-3.64(19)	$\mu^{(0)}_{2466}$	-0.7438(86)
$\mu^{(0)}_{114}$	-5.25(25)	$\mu^{(0)}_{1146}$	3.268(36)	$\mu^{(0)}_{3335}$	-15.18(16)
$\mu^{(0)}_{115}$	-9.84(16)	$\mu^{(0)}_{1155}$	-0.995(35)	$\mu^{(0)}_{3445}$	-0.7453(56)
$\mu^{(0)}_{123}$	1.707(52)	$\mu^{(0)}_{1156}$	6.649(44)	$\mu^{(0)}_{3555}$	-0.6499(73)
$\mu^{(0)}_{124}$	2.4(11)	$\mu^{(0)}_{1222}$	-26.84(74)	$\mu^{(0)}_{3556}$	-0.3512(88)
$\mu^{(0)}_{133}$	12.08(70)	$\mu^{(0)}_{1245}$	2.565(41)	$\mu^{(0)}_{4444}$	-0.0903(26)
$\mu^{(0)}_{136}$	-0.69(11)	$\mu^{(0)}_{1256}$	1.12(35)	$\mu^{(0)}_{4445}$	-0.0542(14)
$\mu^{(0)}_{144}$	-0.6454(55)	$\mu^{(0)}_{1334}$	-4.64(14)	$\mu^{(0)}_{4466}$	-0.0246(13)
$\mu^{(0)}_{146}$	-4.135(22)	$\mu^{(0)}_{1355}$	3.787(34)	$\mu^{(0)}_{4555}$	-0.0704(15)
$\mu^{(0)}_{155}$	-3.868(21)	$\mu^{(0)}_{1366}$	0.518(36)	$\mu^{(0)}_{4556}$	-0.2147(13)
$\mu^{(0)}_{156}$	-6.144(27)	$\mu^{(0)}_{1445}$	0.3319(65)	$\mu^{(0)}_{5666}$	0.0617(15)
$\mu^{(0)}_{223}$	-0.794(34)	rms[b]	0.0006		

[a]Quantities in parentheses are standard errors in units of the last digit given.

[b]Root-mean-square deviation of the fitting in D.

III. COMPUTATIONAL DETAILS

A. Rotation-vibration wavefunctions

We wish to calculate the intensities of electric dipole transitions within the ground electronic state of NH_3. We consider a transition from an initial state i with rotation-vibration wavefunction $|\Phi_{\rm rv}^{(i)}\rangle$ to a final state f with rotation-vibration wavefunction $|\Phi_{\rm rv}^{(f)}\rangle$. As discussed at length in [6], the rotation-vibration wavefunctions $|\Phi_{\rm rv}^{(i)}\rangle$ and $|\Phi_{\rm rv}^{(f)}\rangle$ are obtained, together with the associated rotation-vibration energies, in variational calculations, i.e., by diagonalization of a matrix representation of the rovibrational Hamiltonian. Consequently, the wavefunctions are expressed as linear combinations of basis functions (see Eq. (65) of [6]):

$$|\Phi_{\rm rv}^{(w)}\rangle = \sum_{VK\tau_{\rm rot}} C_{VK\tau_{\rm rot}}^{(w)} \, |J_w \, K \, m_w \, \tau_{\rm rot}\rangle \, |V\rangle, \quad w = i \;\; \text{or} \;\; f, \tag{3.12}$$

where the $C_{VK\tau_{\rm rot}}^{(w)}$ are expansion coefficients, $|J_w \, K \, m_w \, \tau_{\rm rot}\rangle$ is a symmetrized rotational basis function, and the vibrational basis function $|V\rangle$ is given by

$$|V\rangle = \; |n_1\rangle \; |n_2\rangle \; |n_3\rangle \; |n_{\rm b}, l_{\rm b}, \tau_{\rm bend}\rangle \; |n_{\rm i}, J_w, K, \tau_{\rm inv}\rangle. \tag{3.13}$$

All the functions $|n_1\rangle$, $|n_2\rangle$, $|n_3\rangle$, $|n_{\rm b}, l_{\rm b}, \tau_{\rm bend}\rangle$, and $|n_{\rm i}, J_w, K, \tau_{\rm inv}\rangle$, and the quantum numbers labeling them, are defined in detail in [6]: $|n_1\rangle$, $|n_2\rangle$, and $|n_3\rangle$ are one-dimensional Morse oscillator eigenfunctions describing the stretching motion of the XY_3 molecule, $|n_{\rm b}, l_{\rm b}, \tau_{\rm bend}\rangle$ is a symmetrized eigenfunction of the two-dimensional harmonic oscillator modeling the small-amplitude bending motion, and $|n_{\rm i}, J_w, K, \tau_{\rm inv}\rangle$ is a symmetrized inversion basis function obtained by numerical solution of a zero-order inversion Schrödinger equation. All three quantum numbers $\tau_{\rm rot}$, $\tau_{\rm bend}$, and $\tau_{\rm inv}$ assume values of 0 or 1 in such a way that the parity [12, 24] of $|J_w \, K \, m_w \, \tau_{\rm rot}\rangle$ is $(-1)^{\tau_{\rm rot}}$, the parity of $|n_{\rm b}, l_{\rm b}, \tau_{\rm bend}\rangle$ is $(-1)^{\tau_{\rm bend}}$, and the parity of $|n_{\rm i}, J_w, K, \tau_{\rm inv}\rangle$ is $(-1)^{\tau_{\rm inv}}$.

The rotational basis functions $|J_w \, K \, m_w \, \tau_{\rm rot}\rangle$ depend on three Euler angles θ, ϕ, χ [6, 12, 24], these angles define the orientation of the *molecule-fixed axis system xyz* relative to the space-fixed (or laboratory-fixed) axis system XYZ. The xyz axis system follows the rotation of the molecule. In our HBJ-based theory, it is defined in terms of Eckart and Sayvetz conditions [6, 12]; these conditions minimize the coupling between different types of molecular motion, in particular between rotation and vibration.

Each stretching basis function $|n_j\rangle$, $j = 1, 2, 3$, depends on one coordinate $\Delta r_j^\ell = r_j^\ell - r_\mathrm{e}$, where r_j^ℓ is the linearized version [6] of the internuclear distance r_j, and r_e is the equilibrium value of r_j. The bending basis function $|n_\mathrm{b}, l_\mathrm{b}, \tau_\mathrm{bend}\rangle$ depends on the coordinates $(S_{4a}^\ell, S_{4b}^\ell)$, the linearized versions [6] of

$$S_{4a} = \frac{1}{\sqrt{6}}(2\,\alpha_1 - \alpha_2 - \alpha_3), \tag{3.14}$$

$$S_{4b} = \frac{1}{\sqrt{2}}(\alpha_2 - \alpha_3). \tag{3.15}$$

Finally, the inversion basis function $|n_\mathrm{i}, J_w, K, \tau_\mathrm{inv}\rangle$ depends on the HBJ inversion coordinate ρ defined in [6, 25, 26]. In HBJ theory [11], the small-amplitude vibrations [described by the coordinates $(r_1^\ell, r_2^\ell, r_3^\ell, S_{4a}^\ell, S_{4b}^\ell)$ here] are viewed as displacements from a flexible reference configuration replacing the rigid equilibrium structure of customary rotation-vibration theory (see, for example, [3]). For the XY_3 molecules considered here, we define the reference configuration to have three equal, constant bond lengths $r_1 = r_2 = r_3 = r_\mathrm{e}$ and three equal but variable bond angles $\alpha_1 = \alpha_2 = \alpha_3$. Thus, the reference configuration has $\boldsymbol{C}_{3\mathrm{v}}$ or $\boldsymbol{D}_{3\mathrm{h}}$ geometrical symmetry and we define the inversion coordinate ρ as the angle between the C_3 rotational symmetry axis and any one of the N–H bonds as shown in Fig. 1. That is, $0 \le \rho \le \pi$ and the reference configuration is planar for $\rho = \pi/2$.

In the variational calculations the expansions of the kinetic energy factors $G_{\alpha\beta}$ and the pseudo-potential U [6] are taken to 4th order, and the potential energy V is expanded through 6th order. In the numerical integration of the inversion Schrödinger equation a grid of 1000 points is used. The size of the vibrational basis set is controlled by the parameter P_max where

$$P = 2(n_1 + n_2 + n_3) + n_\mathrm{i} + n_\mathrm{b} \le P_\mathrm{max}. \tag{3.16}$$

The matrices are diagonalized with routines from the LAPACK library [27]. Further details can be found in Ref. [6].

B. Line strengths and intensities

In the present work, we neglect hyperfine structure (i.e., the effect of the nuclear spins on the molecular energies). In this approximation, the line strength $S(f \leftarrow i)$ [8, 12, 24] of

the rotation-vibration transition $f \leftarrow i$ is obtained from Eq. (4) of [8]:

$$S(f \leftarrow i) = g_{\rm ns} \sum_{m_f, m_i} \sum_{A=X,Y,Z} \left| \left\langle \Phi_{\rm rv}^{(f)} \; |\bar{\mu}_A| \, \Phi_{\rm rv}^{(i)} \right\rangle \right|^2 \tag{3.17}$$

where $g_{\rm ns}$ is the nuclear spin statistical weight factor [12, 24] and $\bar{\mu}_A$ is the electronically averaged component of the molecular dipole moment along the space-fixed axis $A = X$, Y, or Z. The quantum numbers m_i and m_f are the projections of the total angular momentum, in units of $\hbar$, on the Z axis in the initial and final states, respectively.

The intensity of absorption spectra is determined by the absorption coefficient $\epsilon(\tilde{\nu})$ [12, 24] which depends on the absorption wavenumber $\tilde{\nu}$. If we assume the absorbing molecules to be in thermal equilibrium at an absolute temperature T, the integral of $\epsilon(\tilde{\nu})$ over an absorption line is related to the line strength as

$$\begin{aligned} I(f \leftarrow i) \; &= \; \int_{\rm Line} \epsilon(\tilde{\nu}) \, d\tilde{\nu} \\ &= \; \frac{8\pi^3 N_A \tilde{\nu}_{if}}{(4\pi\epsilon_0) 3hc} \, \frac{{\rm e}^{-E_i/kT}}{Q} \, [1 - \exp(-hc\tilde{\nu}_{if}/kT)] \, S(f \leftarrow i). \end{aligned} \tag{3.18}$$

This expression is valid for the transition from the state i with energy E_i to the state f with energy E_f, where $hc\tilde{\nu}_{if} = E_f - E_i$, N_A is the Avogadro constant, h is Planck's constant, c is the speed of light in vacuum, k is the Boltzmann constant, ϵ_0 is the permittivity of free space, and, finally, Q is the partition function defined as $Q = \sum_j g_j \, \exp(-E_j/kT)$, where g_j is the total degeneracy of the state with energy E_j and the sum runs over all energy levels of the molecule. Experimental values of $I(f \leftarrow i)$ are obtained by numerical integration of experimentally determined $\epsilon(\tilde{\nu})$-values.

A detailed expression for the line strength of an individual rotation-vibration transition within an isolated electronic state of an XY_3 pyramidal molecule is given in Eq. (21) of [8]. This expression is used in the intensity calculations reported in the present work. It is obtained by inserting Eq. (3.12) in Eq. (3.17) and expressing $\bar{\mu}_A$, $A = X$, Y, Z, in terms of $(\bar{\mu}_x, \bar{\mu}_y, \bar{\mu}_z)$, the dipole moment components along the molecule-fixed axes xyz. The line strength is expressed in terms of the vibronic matrix elements $\langle V' \mid \bar{\mu}_\alpha \mid V'' \rangle$, $\alpha = x$, y, z, and in terms of the expansion coefficients $C^{(f)}_{V'K'\tau'_{\rm rot}}$ and $C^{(i)}_{V''K''\tau''_{\rm rot}}$ from Eq. (3.12). The transformation $(\bar{\mu}_X, \bar{\mu}_Y, \bar{\mu}_Z) \rightarrow (\bar{\mu}_x, \bar{\mu}_y, \bar{\mu}_z)$ is carried out by means of standard techniques described, for example, in Chapter 14 of [12]. Examples of the application of these techniques are given for triatomic molecules in [28, 29].

C. The *ab initio* potential energy surface

The calculations of the present work are made with the CBS**-51816 *ab initio* potential energy surface [4, 8, 9]. At the first step towards determining this surface, ATZFc energies were computed for 51816 nuclear geometries at the CCSD(T)/aug-cc-pVTZ level of theory also used in the dipole moment calculations described in Section II A. At 3814 selected nuclear geometries, more accurate energies (CBS+) were determined by extrapolating the CCSD(T) results to the complete basis set limit and including corrections for relativistic effects and core-valence correlation [4]. The differences between the ATZfc and CBS+ energies were fitted by a fifth-order polynomial in geometrically defined, internal coordinates, and the CBS**-51816 surface (which is close to CBS+ quality) was generated by adding corrections, computed from the fifth-order polynomial, to the ATZfc energies at all 51816 grid points. An analytical representation of this surface was obtained by fitting a sixth-order expansion, given in Eq. (57) of [4], through all CBS**-51816 data points. The resulting 196 potential parameters will be published elsewhere [9]; they are presently available from the authors on request. The CBS**-51816 surface provides a complete description of the electronic-ground-state potential energy surface of NH_3 for energies up to 20000 cm^{-1} above equilibrium.

D. The representation of the dipole moment in the xyz axis system

In order to compute the matrix elements $\langle V' \mid \bar{\mu}_\alpha \mid V'' \rangle$ ($\alpha = x, y, z$), that enter into the expression for the line strength in Eq. (21) of [8], we must determine, from the *ab initio* results discussed in Section II A, the dipole moment components $(\bar{\mu}_x, \bar{\mu}_y, \bar{\mu}_z)$ in the molecule-fixed axis system xyz. As discussed extensively in [8], we aim at representing $(\bar{\mu}_x, \bar{\mu}_y, \bar{\mu}_z)$ as expansions with ρ-dependent expansion coefficients

$$\begin{aligned}\bar{\mu}_\alpha(\xi_1^\ell, \xi_2^\ell, \xi_3^\ell, \xi_{4a}^\ell, \xi_{4b}^\ell; \rho) &= \mu_0^\alpha(\rho) + \sum_k \mu_k^\alpha(\rho)\, \xi_k^\ell + \sum_{k\le l} \mu_{kl}^\alpha(\rho)\, \xi_k^\ell\, \xi_l^\ell \\ &+ \sum_{k\le l\le m} \mu_{klm}^\alpha(\rho)\, \xi_k^\ell\, \xi_l^\ell\, \xi_m^\ell + \sum_{k\le l\le m\le n} \mu_{klmn}^\alpha(\rho)\, \xi_k^\ell\, \xi_l^\ell\, \xi_m^\ell\, \xi_n^\ell \ldots \end{aligned} \tag{3.19}$$

in the linearized variables

$$\xi_k^\ell = 1 - \exp(-a\, \Delta r_k^\ell), \quad k = 1, 2, 3, \tag{3.20}$$

$\xi_{4a}^{\ell} = S_{4a}^{\ell}$, and $\xi_{4b}^{\ell} = S_{4b}^{\ell}$. The range parameter a occurs in the analytical representation for the potential energy function [6].

The ρ-dependent functions $\mu_{kl...}^{\alpha}(\rho)$ ($\alpha = x$ or y) in Eq. (3.19) are chosen as

$$\mu_{kl...}^{\alpha}(\rho) = \sum_{s \geq 0} \mu_{kl...}^{\alpha(s)} (\sin\rho_0 - \sin\rho)^s, \quad 0 \leq \rho \leq \pi, \tag{3.21}$$

where we take $\rho_0 = \pi/2$, corresponding to the planar configuration. To represent $\bar{\mu}_z$, we choose

$$\mu_{kl...}^{z}(\rho) = \sum_{s > 0} \mu_{kl...}^{z(s)} (\cos\rho_0 - \cos\rho)^s \text{ for } \frac{\pi}{2} \leq \rho \leq \pi, \tag{3.22}$$

and

$$\mu_{kl...}^{z}(\rho) = -\mu_{kl...}^{z}(\pi - \rho) \text{ for } 0 \leq \rho < \frac{\pi}{2}. \tag{3.23}$$

The dipole moment components $(\bar{\mu}_x, \bar{\mu}_y)$ have E' symmetry in $\boldsymbol{D}_{3h}(M)$, the molecular symmetry group [6, 8, 12, 24] of NH_3, and $\bar{\mu}_z$ has A_2'' symmetry. The irreducible representations of $\boldsymbol{D}_{3h}(M)$ are given in Table 1 of [8] and in Table A-10 of [12]. The functions in Eqs. (3.21)-(3.23) are chosen so as to ensure that $(\bar{\mu}_x, \bar{\mu}_y, \bar{\mu}_z)$ transform correctly under E^* [12, 24], the inversion operation in $\boldsymbol{D}_{3h}(M)$. The transformation properties under the nuclear permutation operations in $\boldsymbol{D}_{3h}(M)$ [12, 24] impose symmetry relations between the expansion parameters $\mu_{kl...}^{\alpha(s)}$ ($\alpha = x$, y, or z) in Eqs. (3.21)-(3.23); these relations have been derived analytically by means of MAPLE VI [30] as described in [8].

We have already expressed the electronically averaged dipole moment in the electronic ground state of NH_3 in the Molecular Bond (MB) representation [Eqs. (2.1)-(2.11) in conjunction with Table I] and we could now, in principle, obtain the dipole moment components $(\bar{\mu}_x, \bar{\mu}_y, \bar{\mu}_z)$ as analytical functions of the coordinates ρ, ξ_1^{ℓ}, ξ_2^{ℓ}, ξ_3^{ℓ}, ξ_{4a}^{ℓ}, and ξ_{4b}^{ℓ} from the expression in Eq. (2.1). However, as detailed in [8], we have chosen instead the conceptually more complicated, but numerically simpler approach of obtaining, at each *ab initio* point, numerical values of $(\bar{\mu}_x, \bar{\mu}_y, \bar{\mu}_z)$ by carrying out, at the *ab initio* point in question, the coordinate transformation from the body-fixed axis system $x'y'z'$ used in the *ab initio* calculation (Section II A) to the xyz axis system. We then determine the values of the expansion parameters $\mu_{kl...}^{\alpha(s)}$ in Eqs. (3.21)-(3.23) by fitting Eq. (3.19) through the computed values of $(\bar{\mu}_x, \bar{\mu}_y, \bar{\mu}_z)$. The expansion parameters $\mu_{kl...}^{x(s)}$ and $\mu_{kl...}^{y(s)}$ in Eq. (3.21) are connected by symmetry relations since $(\bar{\mu}_x, \bar{\mu}_y)$ have E' symmetry in $\boldsymbol{D}_{3h}(M)$, and so these two dipole moment components must be fitted together. The component $\bar{\mu}_z$, with A_2'' symmetry, can be fitted

TABLE II: Dipole moment derivatives for NH_3.

	Exp.[a]	Present work
$(\partial\bar{\mu}_z/\partial S_1)_{\rm eq}$ /D Å^{-1}	−0.29 ±0.03	−0.20
$(\partial\bar{\mu}_z/\partial S_2)_{\rm eq}$ /D	−1.62 ±0.04	−1.51
$(\partial\bar{\mu}_x/\partial S_{3a})_{\rm eq}$ /D Å^{-1}	0.195±0.025	0.22
$(\partial\bar{\mu}_x/\partial S_{4a})_{\rm eq}$ /D	0.366±0.033	0.35

[a]Experimental values from Ref. [31] with experimental uncertainties indicated.

separately. Taking Eq. (3.19) to 6th order, we fitted the 3×14400 *ab initio* data points using 174 parameters for the $\bar{\mu}_z$ component and 271 parameters for $(\bar{\mu}_x, \bar{\mu}_y)$. The rms deviations attained were 0.000076 D and 0.0002 D, respectively.

The equilibrium ATZfc dipole moment in the representation of Eq. (3.19) is $\mu_{\rm e} = 1.5207$ D which can be compared to the *ab initio* value 1.5198 D [4] and the experimental value of (1.561±0.005) D [23].

Koops *et al.* [31] have obtained experimental values for several 'equilibrium' dipole moment derivatives $(\partial\bar{\mu}_\alpha/\partial S_k)_{\rm eq}$, where $\alpha = x$ or z, and S_k is one of the symmetrized coordinates

$$S_1 = \frac{1}{\sqrt{3}}\left(\Delta r_1 + \Delta r_2 + \Delta r_3\right), \tag{3.24}$$

$$S_2 = \frac{1}{\sqrt{3}}\left(\Delta\alpha_1 + \Delta\alpha_2 + \Delta\alpha_3\right), \tag{3.25}$$

$$S_{3a} = \frac{1}{\sqrt{6}}\left(2\Delta r_1 - \Delta r_2 - \Delta r_3\right), \tag{3.26}$$

and S_{4a} given in Eq. (3.14). In Eqs. (3.24)-(3.26), $\Delta r_i = r_i - r_{\rm e}$ and $\Delta\alpha_i = \alpha_i - \alpha_{\rm e}$, $i = 1, 2, 3$, where $\alpha_{\rm e}$ is the equilibrium value of α_i. With the theoretical expressions obtained for $(\bar{\mu}_x, \bar{\mu}_y, \bar{\mu}_z)$ in the present work, we can calculate corresponding theoretical values by utilizing that [6] $\partial r_i^\ell/\partial r_i \to 1$ and $\partial\alpha_i^\ell/\partial\alpha_i \to 1$ when the molecule approaches the equilibrium configuration. The theoretical values for $(\partial\bar{\mu}_\alpha/\partial S_k)_{\rm eq}$ are compared with the experimental results in Table II.

TABLE III: Band centers ν_{fi} and vibrational transition moments μ_{fi} for $^{14}NH_3$.

States		ν_{fi}[a]/cm^{-1}	μ_{fi}/D				
f	i		Obs.	Ref.[b]	Ref. [22]	Ref. [40][c]	Present work
0^-	0^+	0.79	1.47193(1)[d]	[32]	1.536	1.574	1.4564
ν_2^+	0^-	931.64	0.248(7)	[33]	0.269	0.2183	0.2445
ν_2^-	0^+	968.12	0.236(4)	[33]	0.258	0.2075	0.2347
$2\nu_2^+$	0^-	1596.68	0.02036(25)	[34]	0.027	0.0091	0.0202
$2\nu_2^-$	0^+	1882.18	0.003256(21)	[34]	0.007	0.0261	0.0026
$3\nu_2^+$	0^-	2383.36	0.006	[35][e]	0.004	0.0261	0.0054
$3\nu_2^-$	0^+	2895.51	0.0037	[35][e]	0.003	0.0155	0.0027
$4\nu_2^+$	0^-	3461					0.0020
$4\nu_2^-$	0^+	4055					0.0009
ν_1^+	0^-	3335.23	0.0262(1)	[10]	0.029	0.0366	0.0269
ν_1^-	0^+	3337.08	0.0262(1)	[10]	0.029	0.0366	0.0270
$(\nu_1+\nu_2)^+$	0^-	4293.72	0.0079	[36][e]	0.008	0.0067	0.0087
$(\nu_1+\nu_2)^-$	0^+	4320.06	0.0079	[36][e]	0.008	0.0066	0.0083
ν_3^+	0^+	3443.68	0.0182(1)	[10]	0.014	0.0915	0.0128
ν_3^-	0^-	3443.20	0.0182(1)	[10]	0.014	0.0915	0.0128
$(\nu_2+\nu_3)^+$	0^+	4416.91	0.0103	[36][e]	0.010	0.0128	0.0174
$(\nu_2+\nu_3)^-$	0^-	4434.61	0.0103	[36][e]	0.010	0.0127	0.0173
ν_4^+	0^+	1626.28	0.04204(17)	[34]	0.043		0.0585
ν_4^-	0^-	1626.58	0.04204(17)	[34]	0.043		0.0585
$2\nu_4^0+$	0^-	3215.23	0.0920(6)	[10]			0.0073
$2\nu_4^0-$	0^+	3217.59	0.0920(6)	[10]			0.0074
$2\nu_4^{\pm 2,+}$	0^+	3240.18	0.0920(6)	[10]			0.0091
$2\nu_4^{\pm 2,-}$	0^-	3240.82	0.0920(6)	[10]			0.0089
$(\nu_2+\nu_4)^+$	0^+	2540.53	0.001	[35][e]	0.009	0.0077	0.0062
$(\nu_2+\nu_4)^-$	0^-	2585.34	0.001	[35][e]	0.009	0.008	0.0068

[a]Derived from the experimental data collected in Ref. [6].

[b]Reference for the observed value given under the heading 'Obs.'

[c]*Ab initio* predictions, see text.

[d]Experimental uncertainties are given in parentheses (in units of the last digit quoted) where available.

[e]As cited in [40].

IV. APPLICATIONS

A. Transition moments

With the dipole moment components $(\bar{\mu}_x, \bar{\mu}_y, \bar{\mu}_z)$ represented as given in Eq. (3.19) and the vibrational wavefunctions $|\Phi_{\rm vib}^{(w)}\rangle$, $w = i$ or f, given by Eq. (3.12) for $J = 0$, we can

compute the vibrational transition moments defined as

$$\mu_{fi} = \sqrt{\sum_{\alpha=x,y,z} |\langle \Phi_{\rm vib}^{(f)} \mid \bar{\mu}_\alpha \mid \Phi_{\rm vib}^{(i)} \rangle|^2} \tag{4.27}$$

for vibrational transitions in the electronic ground state of $^{14}NH_3$; the matrix elements required are generated by techniques described in [6] for matrix elements of the potential energy function. In calculating the vibrational wavefunctions, we use the *ab initio* potential energy surface CBS**-51816 (Section III C) and a basis set with $P_{\rm max} = 14$ [Eq. (3.16)]. With this basis set, the $J = 0$ matrix blocks corresponding to A and E symmetries in the group $\boldsymbol{D}_{3h}(M)$ have the dimensions $N(A) = 1455$ and $N(E) = 2571$, respectively.

The values of the vibrational transition moments are, to a large extent, determined by the variation of the dipole moment components with the vibrational coordinates. By comparing our theoretical values for the vibrational transition moments to experimental values and other theoretical values available in the literature for $^{14}NH_3$ [10, 22, 23, 32–41], we can assess the quality of the ATZfc dipole moment surface. We make this comparison in Tables III and IV. In these tables, the vibrational states are labeled such that a superscript + indicates the lower (symmetric) inversion component; the upper (antisymmetric) component is indicated by a superscript −. The symmetric and antisymmetric components of the vibrational ground state are labeled 0^+ and 0^-, respectively. In addition to the transition moment values obtained theoretically in the present work, Tables III and IV give the available experimental values and the results of two other theoretical calculations by Marquandt *et al.* [22] and Pracna *et al.* [40], respectively. These latter results are analogous to ours in that they are 'pure' *ab initio* predictions made without fitting to experiment. The work of Pracna *et al.* [40] also contains the results of such fittings, but we present here their 'potential function I' results, obtained directly from *ab initio* data.

Our results agree very satisfactorily with the experimental transition moment values; the over-all agreement is better than that obtained in the two other theoretical calculations [22, 40] considered here. The most remarkable agreement is found for the fundamental transitions in Table III and for transitions to excited inversion states. The inversion motion in NH_3 involves tunneling between two equivalent minima on the potential energy surface and cannot be reasonably modeled by the motion of a one-dimensional harmonic oscillator. It is gratifying that as shown in Tables III and IV, our theoretical model describes well the intensities of transitions involving changes in the excitation of this complex motion, at least

TABLE IV: Band centers ν_{fi} and vibrational transition moments μ_{fi} for $^{14}NH_3$.

States		ν_{fi}[a]/cm^{-1}	μ_{fi}/D				
f	i		Obs.	Ref.[b]	Ref. [22]	Ref. [40][c]	Present work
ν_2^-	ν_2^+	35.69	1.2448(23)[d]	[37]	1.305	1.355	1.2376
$2\nu_2^+$	ν_2^-	629.35			0.557	0.5084	0.5144
$2\nu_2^-$	ν_2^+	949.75	0.285(10)	[38]	0.313	0.2698	0.2855
$3\nu_2^+$	ν_2^-	1416.03	0.0737(16)	[39]	0.089	0.0288	0.0738
$3\nu_2^-$	ν_2^+	1963.08	0.00081(11)	[39]	0.004	0.0416	0.0011
$4\nu_2^+$	ν_2^-	2494			0.012	0.0413	0.0088
$4\nu_2^-$	ν_2^+	3123			0.004	0.0184	0.0013
ν_1^+	ν_2^-	2367.90	0.0040	[39]	0.015	0.0157	0.0002
ν_1^-	ν_2^+	2404.65	0.0040	[39]	0.014	0.0159	0.0008
$(\nu_1+\nu_2)^+$	ν_2^-	3326.39			0.025	0.0337	0.0244
$(\nu_1+\nu_2)^-$	ν_2^+	3387.63			0.024	0.0312	0.0249
ν_3^+	ν_2^+	2511.25	0.02286(29)	[39]	0.010	0.008	0.0177
ν_3^-	ν_2^-	2475.87	0.02286(29)	[39]	0.010	0.008	0.0181
$(\nu_2+\nu_3)^+$	ν_2^+	3484.48			0.020	0.0913	0.0226
$(\nu_2+\nu_3)^-$	ν_2^-	3467.28			0.017	0.0907	0.0196
ν_4^+	ν_2^+	693.85			0.001	0.0022	0.0087
ν_4^-	ν_2^-	659.25			0.001	0.0022	0.0089
$2\nu_4^{\pm 2,+}$	ν_2^+	2307.75	0.00672(15)	[39]			0.0045
$2\nu_4^{\pm 2,-}$	ν_2^-	2273.49	0.00672(15)	[39]			0.0048
$2\nu_4^0+$	ν_2^-	2247.90	0.00085	[39]			0.0036
$2\nu_4^0-$	ν_2^+	2285.16	0.00085	[39]			0.0031
$(\nu_2+\nu_4)^+$	ν_2^+	1608.10	0.0888(12)	[39]	0.044	0.0867	0.0907
$(\nu_2+\nu_4)^-$	ν_2^-	1618.01	0.0843(27)	[39]	0.044	0.0856	0.0879
ν_1^-	ν_1^+	1.06	1.47912(14)	[23]		1.599	1.4626
$2\nu_2^-$	$2\nu_2^+$	284.71	1.02(18)	[41]	0.995	1.047	0.9383
$3\nu_2^+$	$2\nu_2^-$	501.97	1.05(34)	[41]	0.898	0.943	0.8876
$3\nu_2^-$	$2\nu_2^+$	1298.04			0.113	0.083	0.1116
$4\nu_2^+$	$2\nu_2^-$	1580			0.05	0.0112	0.0512
$4\nu_2^-$	$2\nu_2^+$	2458			0.012	0.0454	0.0096
$3\nu_2^-$	$3\nu_2^+$	511.36			1.037	1.039	0.9671
$4\nu_2^+$	$3\nu_2^-$	566.49					0.9933
$4\nu_2^-$	$3\nu_2^+$	1671					0.0343
$4\nu_2^-$	$4\nu_2^+$	593			1.107	1.072	1.0199
ν_3^+	ν_3^-	0.31	1.5094	[23]		1.626	1.4885
ν_4^+	ν_4^-	1.09				1.574	1.4422

[a]Derived from the experimental data collected in Ref. [6]

[b]Reference for the observed value given under the heading 'Obs.'

[c]*Ab initio* predictions, see text.

[d]Experimental uncertainties are given in parentheses (in units of the last digit quoted) where available.

at low and moderate excitation. The transition moment results suggest that the ATZfc *ab initio* dipole moment surface (Section II A) is the most accurate dipole moment surface currently available for NH_3.

B. Intensity simulations

As discussed in Section I, it is desirable to be able to simulate molecular spectra (i.e., to compute transition wavenumbers and intensities) in order to assist their detection and subsequent 'first-principles assignment'. In the present section, we report such simulations for $^{14}NH_3$ absorption bands starting in the lowest vibrational states $0^{\pm}$ and ending in the states $2\nu_2$, ν_4, ν_1, ν_3, and $2\nu_4$. The simulated spectra are drawn as stick diagrams where the height of the stick representing a line is the integrated absorption coefficient from Eq. (3.18). The line strengths entering into this equation are computed from Eq. (21) of [8] with the spin statistical weight factors $g_{\rm ns}$ from Table 2 of [8]. The simulations are made with the ATZfc *ab initio* dipole moment surface (Section II A) and the CBS**-51816 potential energy surface (Section III C). We generate rovibrational wavefunctions with $J \leq 18$ and, in order to make the necessary variational calculations feasible, the size of the vibrational basis set is reduced to $P_{\rm max} = 8$ [Eq. (3.16)] relative to the $P_{\rm max} = 14$ basis set employed for calculating the vibrational transition moments in Section IV A. The largest matrix blocks obtained with the $P_{\rm max} = 8$ basis set are the E symmetry blocks at $J = 18$ with the dimension $N(E)$= 9150.

We compare our theoretical intensities with the results of two recent experimental studies of $^{14}NH_3$ absorption spectra: The $2\nu_2/\nu_4$ bands in the 5–7 μm region [34] and the $\nu_1/\nu_3/2\nu_4/4\nu_2$ bands* near 3 μm [10]. Both spectra have been recorded at the room temperature. The experimental data (wavenumbers and intensities) for the $2\nu_2/\nu_4$ bands, listed in the Appendix of Ref. [34], include 1203 rovibrational transitions between states with $J \leq 16$. The experimental data for the $2\nu_4/\nu_1/\nu_3$ bands are given in Appendix 1 of Ref. [10] and comprise 975 transitions between states with $J \leq 11$. We simulate spectra in the wavenumber regions 1300–2000 cm^{-1} (for the $2\nu_2/\nu_4$ bands) and 3000–3800 cm^{-1} (for the $2\nu_4/\nu_1/\nu_3$ bands) at $T = 275$ K. In computing the integrated absorption coefficient from Eq. (3.18),

* Here, we only discuss the intensities of the vibrational transitions to the ν_1, ν_3, and $2\nu_4$ states; the amount of experimental data available for the $4\nu_2$ band is very limited [10].

we use the partition function value $Q = 1713.33$, which is obtained from the $J \leq 18$ term values calculated variationally below 6000 cm^{-1}, and the spin statistical weight factors for $^{14}NH_3$ from Table 2 of [8]. We assign to each calculated eigenstate the vibrational quantum numbers V and the rotational quantum number K of the basis function with the largest contribution to the eigenfunction, i.e., with the largest value of $|C^{(w)}_{VK\tau_{\rm rot}}|^2$ in Eq. (3.12). We discard transitions for which the calculated value of $I(f \leftarrow i) < 10^{-4}$ cm mol^{-1}. This threshold is much lower than the integrated absorption coefficient of the weakest observed line [a $2\nu_2$ band line with $I(f \leftarrow i) \approx 0.7$ cm mol^{-1}] listed in Refs. [10, 34].

In Figs. 2 and 3 we show simulations of the $2\nu_2$, ν_4, $2\nu_4$, ν_1, and ν_3 absorption bands of $^{14}NH_3$. The bands are artificially separated according to the assignment of the upper state. For example, in the 1300–2000 cm^{-1} wavenumber region (Fig. 2) we plot in separate displays the transitions to the ν_4 and $2\nu_2$ states, respectively. Each simulated band is compared to an 'experimentally derived' stick spectrum drawn with experimental values for transition wavenumbers and intensities taken from Refs. [10, 34]; these transitions are also artificially separated according to the 'experimental' assignment of the upper state. The experimentally derived spectra show only the transitions assigned in [10, 34] and this explains why the experimental spectra generally contain less lines than the simulated ones. In the simulated and the experimentally derived stick spectra, the intensities are given as integrated absorption coefficients in cm mol^{-1}. The experimental values, originally [34] given in cm^{-2} atm^{-1}, were converted to cm mol^{-1} at $T = 295$ K. Note that the same absolute intensity scale is used for the two members of each theoretical/experimental spectrum pair.

It should be mentioned that in the wavenumber intervals 1300–2000 cm^{-1} and 3000–3800 cm^{-1}, there are more vibrational bands than those assigned in [10, 34]. For example, the hot bands $(3\nu_2 - \nu_2)/(\nu_2 + \nu_4 - \nu_2)$ [39] lie in the 5–7 μm region and overlap with the $2\nu_2/\nu_4$ bands. This, of course, makes the experimental assignment more complicated. Also, the 'theoretical assignment' based on the eigenvector coefficients $C^{(w)}_{VK\tau_{\rm rot}}$ in Eq. (3.12) can differ from the 'experimental assignment' in the event of strong accidental mixing of different basis functions in an eigenfunction. However, we do not expect such effects to be very important in the present study as we are not aiming at a line-by-line comparison of theory with experiment, but rather at a qualitative band-structure comparison. Therefore we disregard possible misassignments and plot each simulated band separately as described above.

FIG. 2: Comparison of simulated and observed [34] spectra near 5–7 μm: The ν_4 and $2\nu_2$ absorption bands of $^{14}NH_3$.

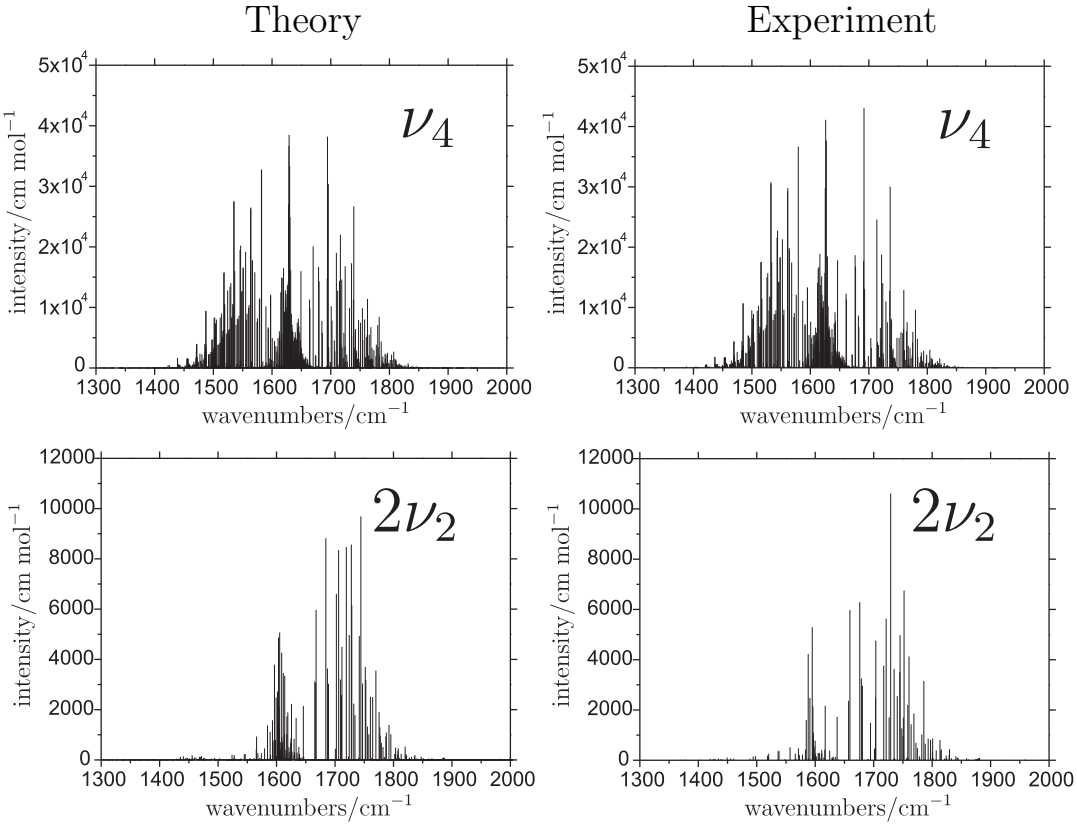

For the $2\nu_2/\nu_4$ band system shown in Fig. 2 there is significant similarity between the simulated and 'experimentally derived' stick spectra, in particular in the case of the ν_4 fundamental band, for which a large amount of experimental data (935 transitions) is available. Also for the $2\nu_4/\nu_1/\nu_3$ band system in Fig. 3 do the simulated fundamental bands ν_1 and ν_3 look highly similar to their experimental counterparts. The similarity is less pronounced for the weaker transitions to the overtone levels $2\nu_4$. It is obvious that for the $2\nu_4$ bands, the experimentally derived stick spectra contain significantly less lines than the simulations, and some of this dissimilarity may be due to the fact that not all $2\nu_4$ lines were assigned in [10], possibly because in the real spectrum, they overlap with stronger ν_1/ν_3 lines. The trend of the vibrational transition moments in Tables III and IV is reflected in the line intensities: The vibrational transition moment of the ν_1 fundamental band is approximately twice as large as the ν_3 transition moment, and therefore the ν_1 band is approximately four times stronger than the ν_3 band.

FIG. 3: Comparison of simulated and observed [10] spectra near 3 μm: The ν_1, ν_3, $2\nu_4^0$, and $2\nu_4^{\pm 2}$ absorption bands of $^{14}NH_3$.

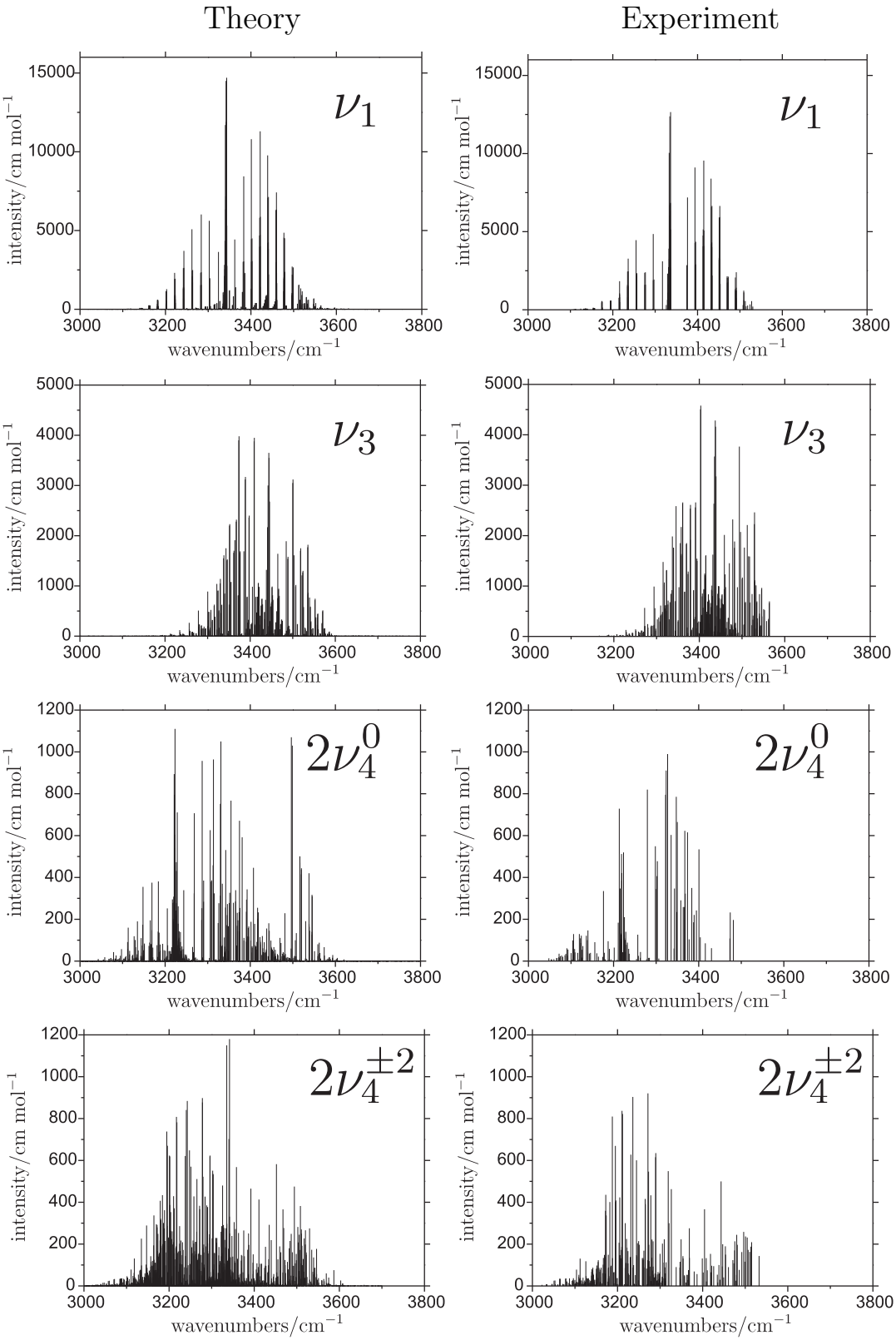

TABLE V: Integrated absorption coefficients I (in $\mathrm{cm}^{-2}\mathrm{atm}^{-1}$) for the strongest rotation-vibration transitions in the ν_4, $2\nu_2$, $2\nu_4$, ν_1, and ν_3 bands of $^{14}NH_3$.[a]

Band	$\Delta J(J_i)$	Γ_f	Γ_i	K_f	K_i	ν_{if}[b]	I(Obs.)[c]	I(Calc.)[d]
ν_4	R(3)	A_2'	A_2''	4	3	1691.73732	1.750	1.551
$2\nu_2$	R(6)	A_2'	A_2''	6	6	1729.03147	0.437	0.394
$2\nu_4^0$	R(4)[e]	A_2''	A_2'	0	0	3271.44070	0.037	0.042
$2\nu_4^{\pm 2}$	R(3)	A_2'	A_2''	4	3	3326.98822	0.040	0.036
ν_1	Q(3)	A_2'	A_2''	3	3	3336.39046	0.514	0.598
ν_3	P(3)	A_2'	A_2''	2	3	3403.38391	0.186	0.160

[a]In the transition labels, J_i, K_i, and Γ_i (J_f, K_f, Γ_f) are the J-value, K-value, and $\boldsymbol{D}_{3h}$(M) rotation-vibration symmetry, respectively, of the initial (final) state. The labels P, Q, R correspond to $\Delta J = J_f - J_i = -1$, 0, and 1, respectively.

[b]Experimentally determined transition wavenumber [10, 34] in cm^{-1}.

[c]Experimentally observed intensity from Refs. [10, 34].

[d]Theoretical intensity from the present work.

[e]The experimental assignment for this $2\nu_4^0$ band line is R(4), $K_i = K_f = 2$ (see text).

In Table V we compare theoretical and experimentally determined values for the integrated absorption coefficients of the strongest rotation-vibration transition in each of the five vibrational bands considered here. Also for these intensities of individual rotation-vibration lines, there is good agreement between theory and experiment. Each of the theoretical intensity values is relatively close to its experimentally observed counterpart. If we sort the lines in Table V in order of increasing intensity, we obtain the sequence $2\nu_4^0 < 2\nu_4^{\pm 2} < \nu_3 < 2\nu_2 < \nu_1 < \nu_4$. Apart from the very small difference in intensity between the $|l_4| = 0$ and 2 components of the $2\nu_4$ band, this sequence is correctly reproduced by the theoretical calculation and reflects the values of the vibrational transition moments in Tables III and IV. The strongest observed line in the $2\nu_4^0$ band [10] has the experimental assignment R(4), $K_i = K_f = 2$ [see footnote a of Table V for the explanation of the transition labels] and the theoretical assignment R(4), $K_i = K_f = 0$. The theoretical calculation, however, produces two lines stronger than this line, namely Q(3), $K_i = K_f = 3$ with I(Calc.) = 0.045 $\mathrm{cm}^{-2}\mathrm{atm}^{-1}$ and R(7), $K_i = K_f = 3$ with I(Calc.) = 0.044 $\mathrm{cm}^{-2}\mathrm{atm}^{-1}$.

In both of the wavenumber regions 1300–2000 cm^{-1} [Fig. 2] and 3000–3800 cm^{-1} [Fig. 3] considered here, the simulations of the weakest bands [$2\nu_2$ in the 1300–2000 cm^{-1} region and $2\nu_4$ in the 3000–3800 cm^{-1} region] show the largest discrepancies from the experimentally

derived stick spectra. The most noticeable discrepancy is that, as mentioned above, for the weak bands the simulated spectra contain significantly more lines than the experimentally derived ones. This indicates that in the weak bands, many lines were not assigned in the experimental studies of Refs. [10, 34] even though their intensities appear significant in our simulations. Since in the experiment, all bands in a given wavenumber region are superimposed, a plausible explanation of the 'extraneous' simulated weak-band lines is that in the observed spectrum, many of these lines overlap with strong-band lines so that it is impossible to assign them.

C. Simplified intensity calculations

The simulations shown in Figs. 2 and 3 are made in an approximation where we aim at high accuracy in each stage of the calculation. We now present the results of calculations where we degrade the accuracy of selected elements of the computational scheme in order to investigate how these elements influence the computed wavenumbers and intensities. We focus on four elements of the calculation:

(a) The basis set. In the 'standard' calculations producing Figs. 2 and 3, we used a basis set with $P_{\max} = 8$ [Eq. (3.16)].

(b) The expansion of the vibrational-coordinate dependent functions $G_{\alpha,\beta}$ [6] in the kinetic energy operator. In the standard calculations, these expansions are truncated after 4th order in the linearized coordinates ξ_n^ℓ, $n = 1, 2, \ldots, 5$.

(c) The expansion of the potential energy function V in terms of the ξ_n^ℓ coordinates, taken to 6th order in the standard calculation.

(d) The expansion of the dipole moment components $\bar{\mu}_\alpha$, $\alpha = x, y, z$ in the ξ_n^ℓ coordinates; these expansions are taken to 6th order in the standard calculation.

In a very crude model for molecular intensities we would describe the rotation of NH_3 as that of a rigid symmetric rotor (taken to be the NH_3 molecule at equilibrium) and the vibrational motion as that of uncoupled harmonic oscillators. That is, the wavefunction would be a product of a rigid-rotor function $|J, k, m\rangle$ [12, 24] and harmonic-oscillator eigenfunctions describing the normal modes of NH_3. Furthermore, the electronically averaged dipole

moment would be represented as a first-order expansion in normal coordinates [12, 24]. In principle, we would like to compare our standard simulations in Figs. 2 and 3 with simulations obtained in this very crude model. However, as remarked in Section III A, it is entirely inappropriate to model the inversion motion by the motion of a harmonic oscillator since the inversion involves the tunneling between two potential minima separated by a superable barrier. Therefore, in degrading the accuracy of the calculations, we maintain the numerically generated inversion basis functions also used in the standard calculations. These can be thought of as *rigid invertor* wavefunctions [25, 26]. We also maintain in the test calculations the Morse-oscillator functions of Section III A as basis functions for the stretching motion, and so, in these calculations, we do not neglect the anharmonicity of the stretching motion.

We make test simulations of the ν_4 and $2\nu_2$ bands at $T = 295$ K by degrading the calculations in the following manner:

(A) *Basis set reduction.* We reduce the basis set to have $P_{\max} = 2$ [Eq. (3.16)]; this is the smallest basis set capable of producing the upper states of the $\nu_4/2\nu_2$ transitions. The simulated spectra, shown in the 'A' displays of Fig. 4, are drastically changed relative to the standard simulations. Both the absolute intensities and the line positions undergo serious changes.

(B) *Simplification of the kinetic energy operator.* To assess the importance of the kinetic energy operator for the quality of the spectrum simulations, we calculate intensities with the vibrational-coordinate-dependent functions $G_{\alpha,\beta}$ in the kinetic energy operator [6] set equal to the zero-order term $G^{(0)}_{\alpha,\beta}(\rho) = G_{\alpha,\beta}(\rho, r_i^\ell = r_\mathrm{e}, \alpha_i^\ell = \alpha_\mathrm{e})$ which depends on ρ only. $G^{(0)}_{\alpha,\beta}(\rho)$ is the value of $G_{\alpha,\beta}$ in the reference configuration. All other aspects of the calculation are kept in their standard form. The resulting simulated spectra are shown in the 'B' displays of Fig. 4. The effect of the kinetic energy simplification is drastic: The simulated $2\nu_2$ band changes so much that it is hardly recognizable and the ν_4 band is also altered significantly from the standard simulation in Fig. 2.

(C) *Simplification of the potential energy function.* We truncate the expression for the potential energy function after the second-order terms in the five linearized coordinates

FIG. 4: The ν_4 and $2\nu_2$ bands of $^{14}NH_3$ simulated at $T = 275$ K with (A) a reduced basis set, (B) a simplified kinetic energy operator, (C) a simplified potential energy function, and (D) a simplified dipole moment representation (see text).

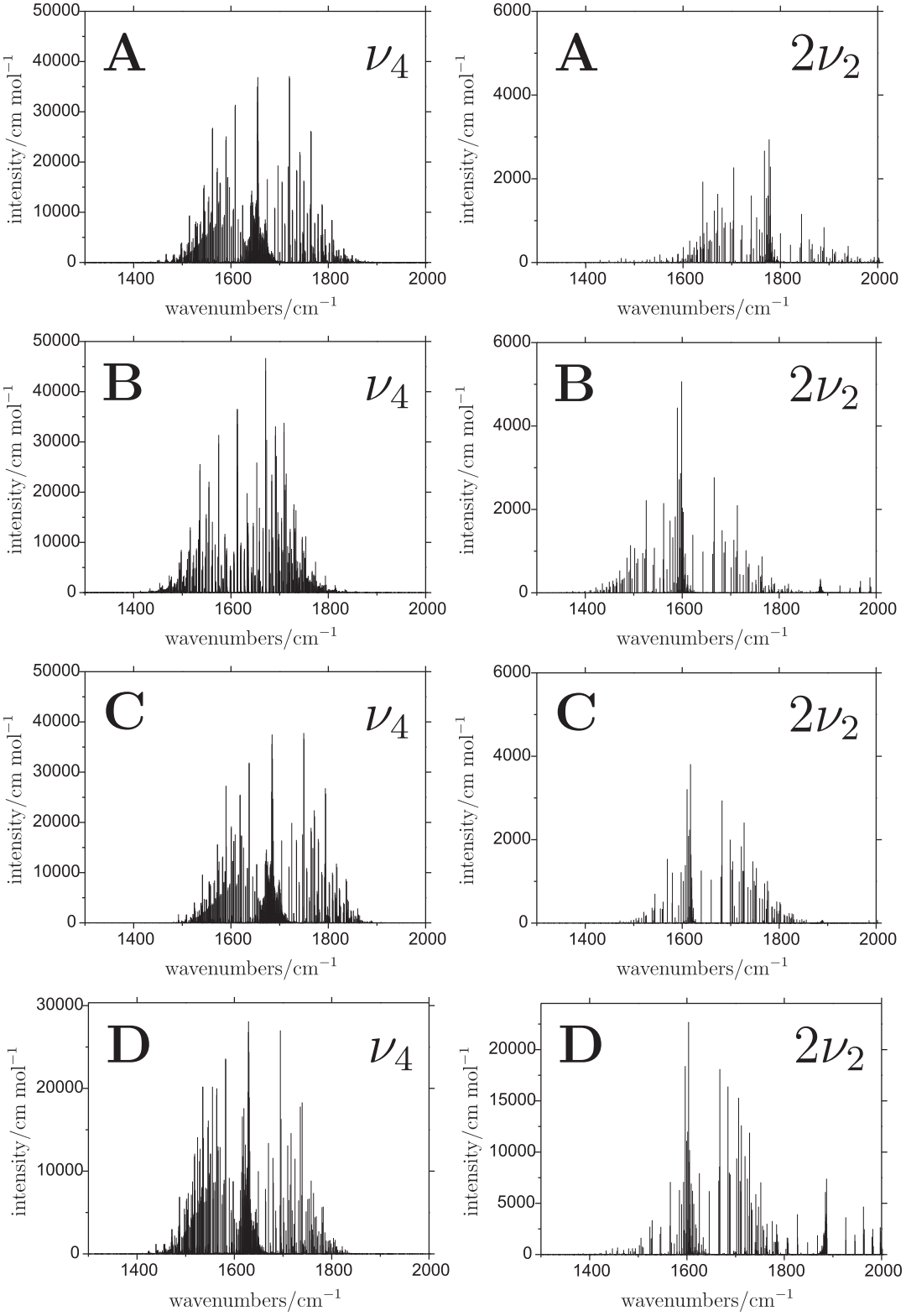

ξ_n^ℓ:

$$V = V^{(0)}(\rho) + \sum_k V_k^{(1)}(\rho)\,\xi_k^\ell + \sum_{kl} V_{kl}^{(2)}(\rho)\,\xi_k^\ell\,\xi_l^\ell \tag{4.28}$$

while keeping the basis set and the functions $G_{\alpha,\beta}$ in their standard forms. The effect of the potential-energy truncation (shown in the 'C' displays of Fig. 4) is noticeable but minor for the ν_4 band while very pronounced in the case of the $2\nu_2$ band.

(D) *Simplification of the dipole moment expansion.* We simplify the analytical representation of the dipole moment components as much as possible by considering only the leading terms in Eq. (3.19):

$$\bar{\mu}_x \;=\; \mu_{4a}^x\,\xi_{4a}, \tag{4.29}$$

$$\bar{\mu}_y \;=\; \mu_{4a}^x\,\xi_{4b}, \tag{4.30}$$

$$\bar{\mu}_z \;=\; \mu_0^z\,\cos\rho; \tag{4.31}$$

all other parameters of the calculation are kept at their standard values. In this rather customary approximation, the ν_4 intensities derive solely from $\bar{\mu}_x$ and $\bar{\mu}_y$, whereas the intensity of the $2\nu_2$ band originates in $\bar{\mu}_z$. The simulated spectra are given in the 'D' displays of Fig. 4. When we compare with the standard results in Fig. 2, there is no noticeable change in the structure of the ν_4 band, except that the intensities are lowered by factor of two. However, the $2\nu_2$ band, whose upper state is an excited inversion state, has completely lost its original structure.

When we compare Figs. 2 and 4, we see that for the ν_4 fundamental band, the degradation of the kinetic energy operator (B) has the largest influence on the intensity pattern. This is to be expected since the ν_4 band is a strong band that remains *allowed* (in the sense of Chapter 12 of [24]) when we make the approximations (A), (C), (D) described above. The much weaker $2\nu_2$ band would be *forbidden* (in the sense of Chapter 12 of [24]) if the vibrational wavefunctions were approximated by those of uncoupled harmonic oscillators and we use first-order expansions of the molecule-fixed molecular dipole moment components. This band is heavily influenced by all four approximations (A)-(D), and so, conversely, in order to obtain a correct description of it we must employ high-level approximations in all stages of the nuclear-motion calculation.

If we make all of the four simplifications (A)-(D) simultaneously, we arrive at a computational scheme similar to the very crude approximation mentioned above, in which we

FIG. 5: A simulation of the ν_4 and $2\nu_2$ bands of $^{14}NH_3$ at $T = 275$ K with all four simplifications (A)-(D) made simultaneously (see text), compared to the standard results.

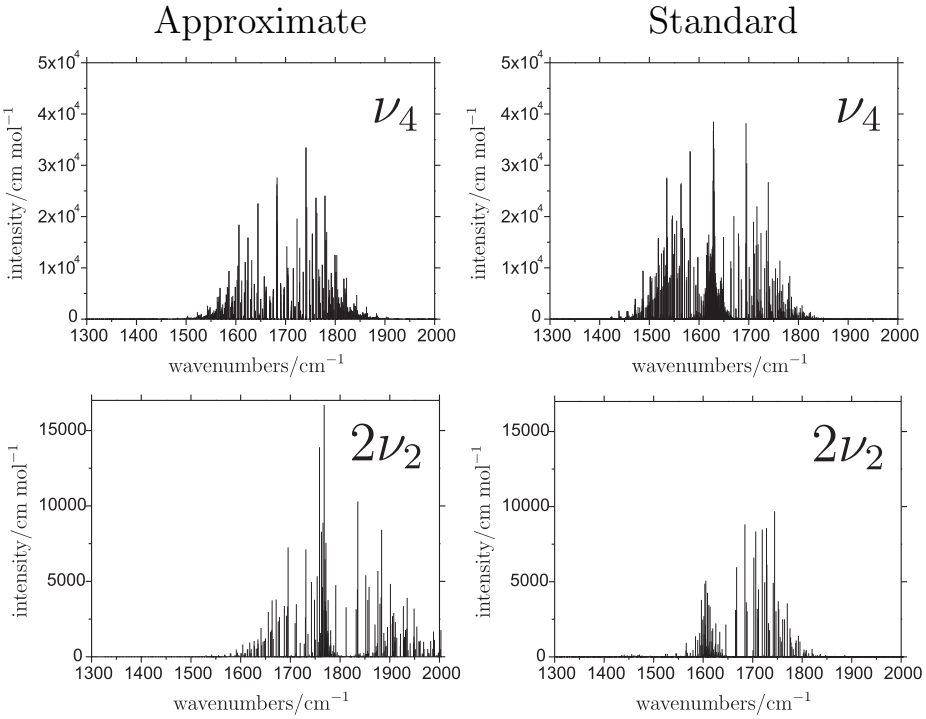

would employ a rigid-rotor-harmonic-oscillator wavefunction and introduce 'electrical harmonicity' by truncating the expansions for the molecule-fixed dipole moment components after the first order terms in the normal coordinates. It should be noted, however, that for the reasons given above, the inversion motion is treated in the rigid invertor approximation [25, 26], and the stretching motion is described by Morse oscillator basis functions which account for anharmonicity. In addition, we cannot quite implement an 'electrically harmonic' dipole moment function here because we express $\bar{\mu}_z$ in terms of the curvilinear coordinate ρ. In the displays headed 'Approximate' in Fig. 5 we plot the simulations of the $2\nu_2/\nu_4$ bands calculated with all the four simplifications (A)-(D); the displays headed 'Standard' are repetitions of the simulations from the standard calculation in Fig. 2. For both bands considered, the combined simplifications (A)-(D) change the simulations very significantly, the effect being by far the largest for the weak $2\nu_2$ band.

V. SUMMARY AND CONCLUSION

We have presented here extensive first-principles simulations of rotation-vibration spectra of $^{14}NH_3$. The calculations are carried by means of recently developed computational methods for calculating rotation-vibration energies and intensities for isolated electronic states of XY_3 pyramidal molecules [6, 8]. By degrading the accuracy of selected elements of the calculations, we have further investigated the influence of customary approximations on the intensity values obtained. The result of these numerical experiments is an illustration of the properties of allowed and forbidden bands as discussed, for example, in Chapter 12 of [24]. The ν_4 band of $^{14}NH_3$ is allowed even in the crude approximation of rigid-rotor/harmonic-oscillator wavefunctions and an 'electrically harmonic' dipole moment function. Therefore, this band is strong and its intensities are relatively insensitive to improvements in the intensity calculation. The $2\nu_2$ band requires 'electrical anharmonicity' (i.e., an expansion of the dipole moment at least to second order in the normal coordinates) to gain intensity. It is forbidden in the crude approximation of rigid-rotor/harmonic-oscillator wavefunctions and an 'electrically harmonic' dipole moment function. Consequently it is much weaker than the ν_4 band, and its intensity pattern is crucially dependent on the level of theory in the nuclear-motion calculation.

As witnessed by the vibrational transition moments in Tables III and IV, the simulated spectra in Figs. 2 and 3, and the line strengths of individual rotation-vibration transitions in Table V, the theoretical intensity results of the present work are generally in very satisfactory agreement with the experimentally measured intensity values available for the electronic ground state of $^{14}NH_3$. Not only do we predict vibrational transition moments that explain the relative intensities of the observed vibrational bands, we also compute absolute line-strength values for individual rotation-vibration lines in good agreement with experimental results. Consequently, we expect that our computational method, in conjunction with high-quality *ab initio* potential energy and dipole moment surfaces, can simulate rotation-vibration spectra of XY_3 pyramidal molecules prior to observation with sufficient accuracy to facilitate the observation and assignment of these spectra.

Acknowledgements

The initial stages of this work were supported by the European Commission through contract no. HPRN-CT-2000-00022 "Spectroscopy of Highly Excited Rovibrational States". The work of PJ is supported in part by the Deutsche Forschungsgemeinschaft and the Fonds der chemischen Industrie.

---

[1] S. V. Shirin, O. L. Polyansky, N. F. Zobov, P. Barletta, and J. Tennyson, *J. Chem. Phys.*, **118**, 2124 (2003)

[2] O. L. Polyansky, A. G. Császár, S. V. Shirin, N. F. Zobov, P. Barletta, J. Tennyson, D. W. Schwenke, and P. J. Knowles, *Science*, **299**, 539 (2003)

[3] D. Papoušek and M. R. Aliev, *Molecular Vibrational-Rotational Spectra*, Elsevier, Amsterdam, 1982.

[4] H. Lin, W. Thiel, S. N. Yurchenko, M. Carvajal, and P. Jensen, *J. Chem. Phys.*, **117**, 11265 (2002)

[5] S. N. Yurchenko, M. Carvajal, P. Jensen, F. Herregodts, and T. R. Huet, *Chem. Phys.*, **290**, 59 (2003)

[6] S. N. Yurchenko, M. Carvajal, Per Jensen, Hai Lin, J. Zheng, and W. Thiel, *Mol. Phys., in press.*

[7] S. N. Yurchenko, W. Thiel, S. Patchkovskii, and P. Jensen, *Phys. Chem. Chem. Phys., submitted for publication.*

[8] S. N. Yurchenko, M. Carvajal, W. Thiel, H. Lin, and P. Jensen, *Adv. Quant. Chem., in press.*

[9] H. Lin, J. J. Zheng, S. N. Yurchenko, P. Jensen, and W. Thiel, in preparation.

[10] I. Kleiner, L. R. Brown, G. Tarrago, Q.-L. Kou, N. Picqué, G. Guelachvili, V. Dana, and J.-Y. Mandin, *J. Mol. Spectrosc.*, **193**, 46 (1999)

[11] J. T. Hougen, P. R. Bunker, and J. W. C. Johns, *J. Mol. Spectrosc.*, **34**, 136 (1970)

[12] P. R. Bunker and P. Jensen, *Molecular Symmetry and Spectroscopy*, 2nd ed. NRC Research Press, Ottawa, 1998.

[13] P. Jensen, G. Osmann, and I. N. Kozin, in: "Vibration-Rotational Spectroscopy and Molecular Dynamics" (D. Papoušek, Ed.), World Scientific, Singapore, 1997.

[14] MOLPRO2000 is a package of *ab initio* programs written by H.-J. Werner and P. J. Knowles, with contributions from R. D. Amos, A. Bernhardsson, A. Berning *et al.*

[15] C. Hampel, K. Peterson, and H.-J. Werner, Chem. Phys. Lett. **190**, 1 (1992), and references therein. The program to compute the perturbative triples corrections has been developed by M. J. O. Deegan and P. J. Knowles, *ibid.* **227**, 321 (1994).

[16] G. D. Purvis and R. J. Bartlett, *J. Chem. Phys.*, **76**, 1910 (1982)

[17] M. Urban, J. Noga, S. J. Cole, and R. J. Bartlett, *J. Chem. Phys.*, **83**, 4041 (1985)

[18] K. Raghavachari, G. W. Trucks, J. A. Pople, and M. Head-Gordon, *Chem. Phys. Lett.*, **157**, 479 (1989)

[19] T. H. Dunning, *J. Chem. Phys.*, **90**, 1007 (1989)

[20] D. E. Woon and T. H. Dunning, *J. Chem. Phys.*, **98**, 1358 (1993)

[21] S.-G. He, J.-J. Zheng, S.-M. Hu, H. Lin, Y. Ding, X.-H. Wang, and Q.-S. Zhu, *J. Chem. Phys.*, **114**, 7018 (2001)

[22] R. Marquardt, M. Quack, I. Thanopulos, and D. Luckhaus, *J. Chem. Phys.*, **119**, 10724 (2003)

[23] M. D. Marshall, K. C. Izgi, and J. S. Muenter, *J. Chem. Phys.*, **107**, 1037 (1997)

[24] P. R. Bunker and P. Jensen, *Fundamentals of Molecular Symmetry*, IOP Publishing, Bristol, 2004.

[25] D. Papoušek, J. M. R. Stone, and V. Špirko, *J. Mol. Spectrosc.*, **48**, 17 (1973)

[26] V. Špirko, *J. Mol. Spectrosc.*, **101**, 30 (1983)

[27] E. Anderson, Z. Bai, C. Bischof, S. Blackford, J. Demmel, J. Dongarra, J. Du Croz, A. Greenbaum, S. Hammarling, A. McKenney, and D. Sorensen, LAPACK Users' Guide, http://www.netlib.org/lapack/, Third Edition, 1999.

[28] P. Jensen and V. Špirko, *J. Mol. Spectrosc.*, **118**, 208 (1986)

[29] P. Jensen, *J. Mol. Spectrosc.*, **132**, 429 (1988)

[30] M. B. Monagan, K. O. Geddes, K. M. Heal, G. Labahn, S. M. Vorkoetter, and J. McCarron, Maple 6 Programming Guide, Waterloo Maple, Toronto, 2000.

[31] T. Koops, T. Visser, and W. M. A. Smit, *J. Mol. Structure*, **96**, 203 (1983) (????)

[32] K. Tanaka, H. Ito, and T. Tanaka, *J. Chem. Phys.*, **87**, 1557 (1987)

[33] T. Nakanaga, S. Kondo, and S. Saëki, *J. Mol. Spectrosc.*, **112**, 39 (1985)

[34] C. Cottaz, G. Tarrago, I. Kleiner, L. R. Brown, J. S. Margolis, R. L. Poynter, H. M. Pickett, T. Fouchet, P. Dorssart, and E. Lellouch, *J. Mol. Spectrosc.*, **203**, 285 (2000)

[35] W. S. Benedict, E. K. Plyler, and E. D. Tidwell, *J. Chem. Phys.*, **29**, 829 (1958)

[36] J. S. Margolis and Y. Y. Kwan, *J. Mol. Spectrosc.*, **50**, 266 (1974)

[37] Y. Ueda and J. Iwahori, *J. Mol. Spectrosc.*, **116**, 191 (1986)

[38] P. H. Beckwith, D. J. Danagher, and J. Reid, *J. Mol. Spectrosc.*, **121**, 209 (1987)

[39] C. Cottaz, G. Tarrago, I. Kleiner, and L. R. Brown, *J. Mol. Spectrosc.*, **209**, 30 (2001)

[40] P. Pracna, V. Špirko, and W. P. Kraemer, *J. Mol. Spectrosc.*, **136**, 317 (1989)

[41] M. Takami, H. Jones, and T. Oka, *J. Chem. Phys.*, **70**, 3557 (1979)